Bulletin of Engineering Geology and the Environment (2020) 79:2483–2498
https://doi.org/10.1007/s10064-019-01710-z

ORIGINAL PAPER

A numerical study to investigate the influence of surface roughness and boundary condition on the shear behaviour of rock joints

Mahdi Saadat[1] · Abbas Taheri[1]

Received: 22 August 2019 / Accepted: 16 December 2019 / Published online: 3 January 2020

Abstract

The shear behaviours of rock joints with and without rock bolt support are numerically studied using the discrete element code PFC2D. A cohesive contact model was employed to reproduce the damage response of the synthetic intact rock (i.e. asperity degradation). We used the smooth-joint model to simulate the micro-scale roughness of the joint surface. We calibrated and validated the proposed numerical framework against the experimental results. A series of numerical constant normal stiffness (CNS) direct shear tests were conducted on idealised and natural rock joints to investigate the influence of the boundary condition on the shear behaviour of rock joints. In particular, the importance of CNS condition, surface roughness, asperity angle, and the initial normal stress were studied. Additionally, the shear and damage mechanism of bolted rock joints under constant normal load (CNL) and CNS condition was numerically investigated. The results presented show that the shear resistance of the joint increases under both CNL and CNS conditions, but at a high degree of roughness, no significant enhancement was observed on the value of peak shear stress.

Keywords DEM simulation · Constant normal stiffness · Asperity damage · Bolted rock joint · Roughness

Introduction

The natural discontinuities around orebodies can have a profound impact on the stability and safety of mining excavations (Taheri and Tani 2010; Tang et al. 2016; Wang et al. 2019; Wang et al. 2018). Any damage due to roof collapse or rock slope failure can hinder the mining activities and impose penalties to mining companies (Saadat and Taheri 2019b). In this regard, an accurate estimation of rock joint shear response is essential when designing the surface and underground mining structures. Conducting direct shear test is a standard experimental methodology to evaluate the shear behaviour of rock joints. Constant normal load/stress (CNL) and constant normal stiffness (CNS) conditions are two different types of boundary condition that are widely used in direct shear testing of rock joints (Indraratna et al. 2015; Park et al. 2013; Shrivastava and Rao 2018). In the slope stability analysis where the unstable rock block is sliding along the surface of discontinuity without any restriction, CNL boundary condition should be used. In contrast, in underground mining where neighbouring rock blocks restrict the unstable rock block, the applied normal stress is not constant and the analysis of the rock joint requires CNS condition (Bewick et al. 2014; Indraratna and Welideniya 2003; Shang et al. 2018c; Thirukumaran et al. 2016).

In order to reinforce the unstable blocks, the common stabilisation method is to install grouted rock bolts. In general, bolted rock joints are subjected to pull-out and shear loading (Chen and Li 2015b; Srivastava and Singh 2015; Wu et al. 2018). Dey (2001) conducted a series of experimental CNS direct shear tests on bolted rock joints and studied the influence of rock bolt profile on the shear resistance of rock joints. The recent experimental observations of Wu et al. (2018) and Chen et al. (2018) revealed that the surface roughness has a significant contribution to the overall shear performance of bolted rock joints. Previous researchers highlighted the importance of other parameters on shear behaviour of bolted rock joints, including rock strength (Chen and Li 2015a; Jalalifar et al. 2006), rock bolt properties (Chen and Li 2015b; Jalalifar and Aziz 2010; Spang and Egger 1990), and pre-existing flaws (Li et al. 2016c; Zhang et al. 2016).

✉ Mahdi Saadat
mahdi.saadat@adelaide.edu.au

[1] School of Civil, Environmental and Mining Engineering, The University of Adelaide, Adelaide, Australia

Although laboratory testing is the most common approach for investigating the shear mechanism of bolted as well as unbolted rock joints, setting up experiments is expensive and time-consuming. Experimental investigations require researchers to generate a wide range of specimens using various materials, using advanced laboratory equipment. Consequently, some researchers have made their effort to develop numerical models to investigate the shear mechanism of bolted rock joints. Numerical simulations are more efficient and repeatable. Finite element method (FEM) has been used to simulate the shear behaviour of different types of rock bolts and their rupture behaviour (e.g. Grasselli (2005); Jalalifar et al. (2006)), and Li et al. (2016a) used finite difference codes and examined the influence of rock strength, bolt inclination angle, and diameter of rock bolt on the level of bolt resistance. Influence of surface roughness, however, is overlooked in most of the studies. Using finite difference codes, Lin et al. (2014) constructed an idealised saw-tooth rock joint reinforced by rock bolt and conducted a numerical study to investigate the influence of bolt inclination angle on the overall shear strength of bolted rock joints. However, due to the linear elastic nature of their numerical model, the effects of asperity degradation and fracturing in rock specimens were neglected. Liu et al. (2017) and Ghadimi et al. (2015) proposed an analytical model to evaluate the load transfer mechanism of bolted rock joints. However, their study was limited to smooth rock joints without taking into account the influence of surface roughness and CNS condition.

The previous experimental and numerical studies have identified some of the key characteristics of bolted rock joints. However, the evaluation of the shear mechanism of bolted rock joints still requires more quantifications. The rapid growth of numerical modelling has provided an alternative tool for researchers to study the shear behaviour of rock joints by simulating CNL and CNS direct shear tests. Discrete element method (DEM) is proven to be a promising numerical technique to investigate rock and rock joint behaviours (Asadi et al. 2012; Asadi et al. 2013; Bi et al. 2019; Cao et al. 2018a; Cao et al. 2018b; Ghazvinian et al. 2012; Kazerani et al. 2012; Marczewska et al. 2016; Park and Song 2009; Shang et al. 2018b). In this regard, the explicit DEM code, PFC2D (Itasca 2016), has been used to simulate the asperity damage and failure behaviour of rock joints (Bahaaddini et al. 2015; Bahaaddini et al. 2013; Gutiérrez-Ch et al. 2018). In PFC, a dense assembly of DEM particles bonded together at their contact level represents the intact rock. The force-displacement relationships of the contacts are defined at the microscopic scale that can mimic the contact behaviour under mode I, II, and mixed mode loading. The initiation and coalescence of micro-cracks due to bond-break (contact failure) result in the evolution of macroscopic fractures (i.e. asperity damage) in the synthetic rock. The collective response of the particle assembly can be monitored as macroscopic behaviour of the synthetic specimen (i.e. stress-displacement curve).

In the present study, the DEM code available in PFC2D software (Itasca 2016) is employed to investigate the shear behaviour of bolted and unbolted rock joints under CNS condition. A new cohesive model proposed by Saadat and Taheri (2019d) is implemented in the DEM codes to mimic the micro-cracking behaviour of intact rock. We successfully employed the cohesive model in our previous rock joint and rock bolt investigations (Saadat and Taheri 2019a, 2019b). The smooth-joint model (Itasca 2016) is adapted to model the rock joint interface. The potential of the proposed DEM framework is investigated by calibrating and comparing the results of CNL direct shear test on saw-tooth rock joints with experimental counterparts. A series of numerical CNS direct shear tests are conducted on unbolted and bolted rock joints to investigate the influence of CNS boundary condition on asperity damage and shear mechanism of rock joints.

Constitutive relationships

The proposed cohesive model

In the present study, a new cohesive, contact model (CCM) developed by Saadat and Taheri (2019e) was employed for simulating the failure behaviour of rock-like specimens (i.e. asperity damage). There are different DEM contact models available in the literature (e.g. Le et al. (2017); Nguyen et al. (2017a); Nguyen et al. (2017b); and Le et al. (2018)). However, in the CCM the number of micro-mechanical properties was reduced to simplify the calibration procedure and enhance the numerical efficiency. The details of the proposed cohesive contact model can be found in (Saadat and Taheri 2019e). Here, we briefly introduce the formulation of the model:

In the proposed cohesive model, the relative displacement $\boldsymbol{u}(u_n, u_s)$ of the DEM contacts is decomposed into elastic and plastic displacements, which represent the reversible and irreversible displacements:

$$\boldsymbol{u} = \boldsymbol{u}^e + \boldsymbol{u}^p \tag{1}$$

Considering k_n^0 as k_s^0 as normal and shear stiffness of the DEM contacts, the corresponding contact stresses can be calculated as:

$$\sigma_n = k_n^0\left(u_n - u_n^p\right) \tag{2}$$

$$\sigma_s = k_s^0\left(u_s - u_s^p\right) \tag{3}$$

where σ_n and σ_s are normal and shear stresses in the DEM contacts; u_n and u_n^p are the total and plastic normal displacements; u_s and u_s^p are the total and plastic shear displacements.

In order to take into account the mixed-mode failure response of DEM contacts, the following yield function was

proposed:

$$F(\sigma_n, \sigma_s, C) = \sigma_s + \mu\sigma_n - C = 0 \tag{4}$$

This yield function allows us to identify the yield point at which the DEM contact enters its softening stage. μ is the friction coefficient of the contact and C is defined as:

$$C = C^0 e^{-\kappa \iota^p} \tag{5}$$

C^0 is the initial cohesion of DEM contact, κ is a micro-mechanical parameter that accounts for softening response of the contact after yield, and ι^p is the accumulative plastic displacement of the contact, which can be determined from normal and shear increments as:

$$d\iota^p = \sqrt{\left(d\iota_n^p\right)^2 + \left(d\iota_s^p\right)^2} \tag{6}$$

The degree of damage in the cohesive contacts is simply measured using the following equation:

$$D = \frac{C^0 - C}{C^0} = 1 - e^{-\kappa \iota^p} \tag{7}$$

When the DEM contact is bonded and experience no failure $D = 0.0$, when the DEM contact is completely damaged $D = 1.0$, and when the DEM contact is in its softening stage $0.0 \le D \le 1.0$. The details of the stress-return algorithm can be found in our previous studies (Saadat and Taheri 2019a, 2019d).

Figure 1 illustrates the behaviour of DEM contact in mode I and II. The linear elastic portion of stress-displacement curves defines the contact behaviour before failure ($D = 0.0$), followed by a non-linear stage that represents contact softening due to the progressive degradation of cohesion ($0.0 < D < 1.0$). The details of updating the force-displacement law are provided in Saadat and Taheri (2019e). In Fig. 1 C^0 is the cohesion of contacts and μ is the friction coefficient of the contacts. In tension, when the normal stress of the DEM contacts reaches $\frac{C^0}{\mu}$, they enter to their softening stage until complete cohesion degradation ($D = 1.0$). Similarly, during contact shear behaviour, when the maximum shear stress of the contacts is achieved (C^0) their softening response begins until complete cohesion degradation ($D = 1.0$).

Potyondy and Cundall (2004) proposed a deformability method, in which the normal stiffness of the bonds (k_n^0) can be linked to their elastic modulus ($\boldsymbol{E^0}$) as follows (Itasca 2016):

$$k_n^0 = \frac{\boldsymbol{E^0}}{L} \tag{8}$$

where L can be determined as follows:

$$L = \begin{cases} R^1 + R^2, ball-ball \\ R^1 \quad\quad , ball-facet \end{cases} \tag{9}$$

During the calibration process, normal to shear stiffness ratio (k_n^0 / k_s^0) was chosen to approximate the shear stiffness of the contacts ($\overline{k}^s$) (Hofmann et al. 2015; Liu et al. 2018). For calibration purposes, the user can alter the contact stiffnesses after assigning $\boldsymbol{E^0}$ (Itasca 2016). We successfully followed this approach in our previous studies (Saadat and Taheri 2019a, 2019b, 2019c, 2019d, 2020).

The smooth-joint model

The smooth-joint model (SJM) simulates the micro-cracking behaviour of an interface in PFC software (Itasca 2016). The smooth-joint model is an interface model that can be used both

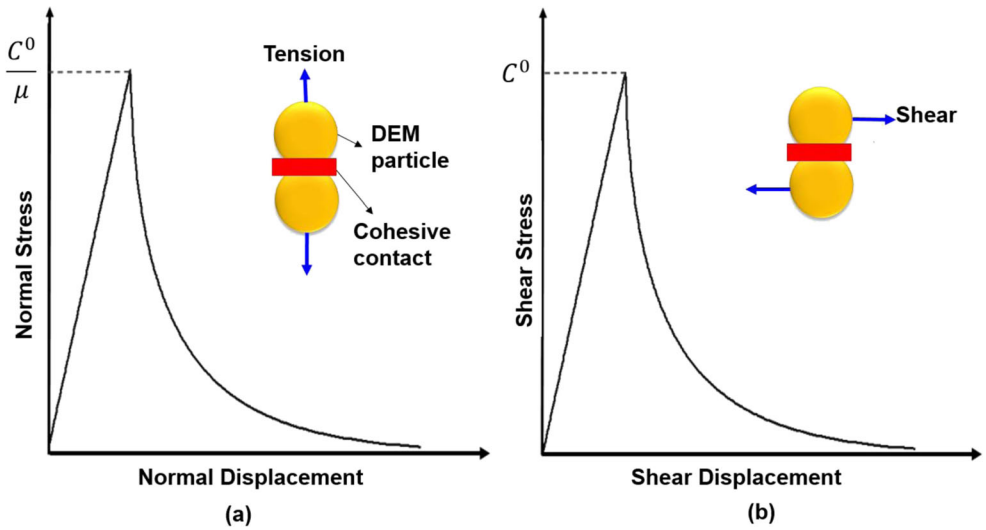

Fig. 1 Stress-displacement behaviour of the proposed cohesive model (a) mode I, and (b) mode II (Saadat and Taheri 2019e)

for small displacement such as simulating grain boundaries in grain-based approach (Saadat and Taheri 2019c, 2019d, 2020), and large displacement such as rock joint interface (Bahaaddini et al. 2013). The SJM is assigned to the DEM contacts representing the interface between two particles. The particles can overlap and pass through each other in this model. Figure 2 illustrates the performance of the SJM installed on the contacts between two DEM particles. In 2D, the orientation of the interface is defined as:

$$\hat{\boldsymbol{n}}_j = \left(\sin\theta_p, \cos\theta_p\right) \tag{10}$$

In Eq. 8, θ_p is the dip angle of the interface. $\hat{\boldsymbol{n}}_c$ in Fig. 2 represents the unit normal vector between two bonded DEM particles. The SJM interface consists of two surfaces (shown as surface 1 and 2 in Fig. 2). If and only if $\hat{\boldsymbol{n}}_j.\hat{\boldsymbol{n}}_c \geq 0$, then particle 2 lies in surface 2. Once the SJM is installed on the interface contacts, the existing bond between DEM particles will be removed and a set of elastic springs will be assigned over a rectangular shapes cross-section. According to Itasca (2016), the cross-sectional area of an interface contact is:

$$\boldsymbol{A} = 2\overline{\boldsymbol{R}}\boldsymbol{t} \tag{11}$$

where t and $\overline{R}$ are the thickness ($t = 1.0$) and radius of smooth-joint model crass-section, respectively. Note that $\overline{R} = \lambda \min\left(R^1, R^2\right)$, where R^1 and R^2 are particles radii, and λ is radius multiplier which is usually taken as 1.0.

The force-displacement law of the SJM is briefly described here:

$$\mathbf{F} = -\boldsymbol{F}_n\hat{\boldsymbol{n}}_j + \mathbf{F_s} \tag{12}$$

The normal force is updated as follows:

$$\boldsymbol{F}_n = (\boldsymbol{F}_n)_0 + \overline{\boldsymbol{k}}_n \boldsymbol{A}\Delta\delta_n^e \tag{13}$$

$(F_n)_0$ is the SJM normal force at the beginning of the timestep, $\overline{k}_n$ is the normal stiffness, $\boldsymbol{A}$ is the contact cross-sectional area, and $\Delta\delta_n^e$ is the normal displacement increment. The trial shear force is calculated as:

$$\mathbf{F}_s^* = (\mathbf{F_s})_0 - \overline{\boldsymbol{k}}_s \boldsymbol{A}\Delta\delta_s^e \tag{14}$$

where $(\mathbf{F_s})_0$ is the shear force at the beginning of the numerical timestep, $\overline{k}_s$ is the shear stiffness, and $\Delta\delta_s^e$ is the shear displacement increment. The shear strength of the SJM contact is assumed as $F_s^\mu = -\mu^{sj} F_n$, where μ^{sj} is the friction coefficient of the bond (particle interface). The micro-mechanical parameters that simulate the contact strength are tensile strength (σ_c) and cohesion (c). The shear strength of the contact is determined from simple Mohr-Coulomb ($\tau_c = \sigma_c \tan(\varphi) + c$). The force-displacement law for a bonded contact is illustrated in Fig. 3. When the bond is not in tension, the shear force is limited by:

$$\mathbf{F_s} = \begin{cases} \mathbf{F}_s^* & , \left\|\mathbf{F}_s^*\right\| < F_s^\mu \\ F_s^\mu \left(\mathbf{F}_s^* \Big/ \left\|\mathbf{F}_s^*\right\| \right) & , \text{otherwise} \end{cases} \tag{15}$$

If $F_n \geq \sigma_c A$, then the contact failure occurs in tension mode (Fig. 3a) and $F_n = |\mathbf{F_s}| = 0.0$; otherwise if $\left|\mathbf{F}_s^*\right| \geq \tau_c A$ the bond breaks in shear mode, and its shear force of is updated by Eq. 13 (Figure 3b).

Calibration and validation of the proposed DEM framework

The micro-mechanical parameters of the proposed cohesive model and the smooth-joint model were calibrated against the experimental data. The details of the calibration procedure and the list of micro-mechanical parameters are provided in our previous research (Saadat and Taheri 2019b). Here, we briefly introduce the calibration results and the list of calibrated micro-properties.

Calibration of the CCM

The micro-mechanical parameters of the CCM were calibrated against the experimental data from UCS test. A numerical

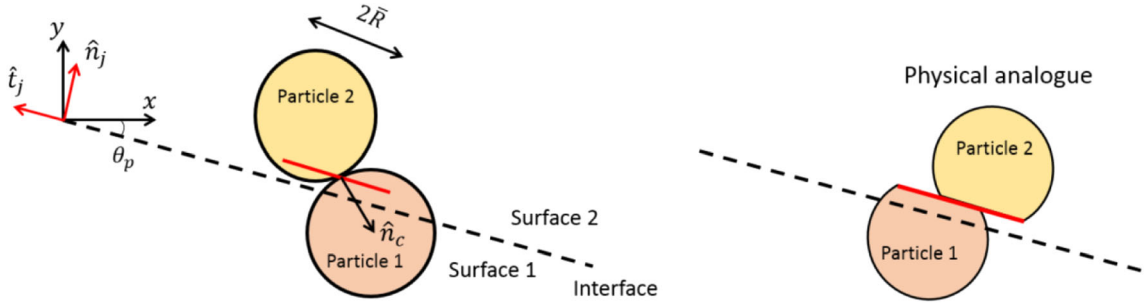

Fig. 2 The smooth-joint model application in PFC2D (modified from Itasca (2016))

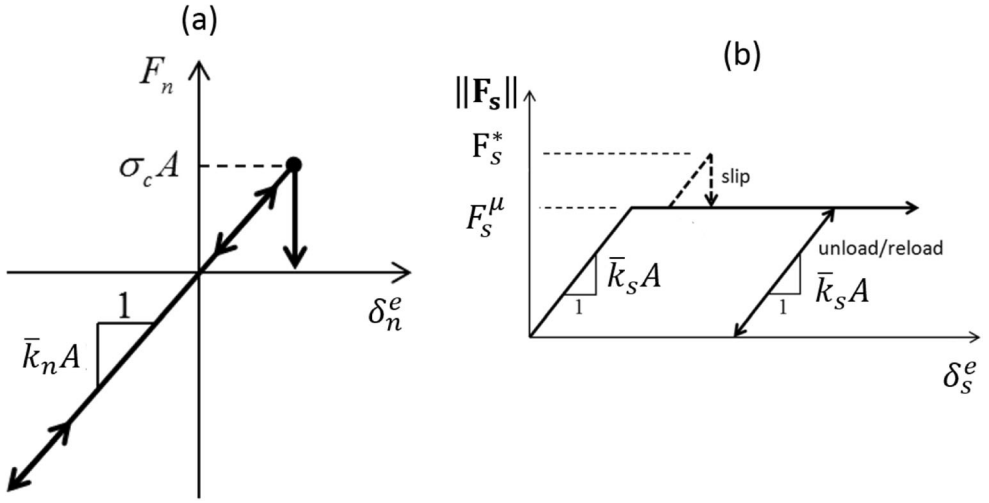

Fig. 3 Force-displacement law in the SJM. (a) Tension mode: normal force versus normal displacement; (b) Shear mode: shear force versus shear displacement (modified from Itasca (2016))

specimen with a height of 100 mm and a width of 40 mm was produced and inverse calibration procedure was adopted to achieve the micro-properties. The minimum particle radius ($R_{\min}$) was chosen to be 0.25 mm, and the ratio of the maximum particle radius to minimum particle radius ($^{R_{\max}}/_{R_{\min}}$) was set as 1.66. The density of DEM particles was 2500 $^{\mathrm{kg}}/_{\mathrm{m}^3}$. In the present study, we adopted global damping of 0.7 suggested by Potyondy and Cundall (2004) for dissipating the kinetic energy. The details of kinetic energy dissipation and damping mechanism can be found in Potyondy and Cundall (2004). Figure 4 illustrates the comparison between the results of the proposed cohesive model and laboratory counterparts. You can see that a good agreement was achieved between numerical and laboratory results. The calibrated micro-properties of the CCM are given in Table 1, and the comparison between macroscopic parameters of the numerical and physical specimens is provided in Table 2. The numerical simulation results are in an excellent agreement with the laboratory data, which demonstrates the capability of the proposed cohesive DEM framework in reproducing the mechanical behaviour of the physical specimen.

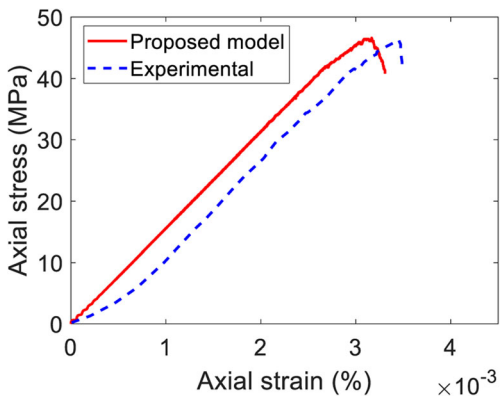

Fig. 4 Calibration of the proposed cohesive model to the laboratory specimen under UCS test

Calibration of the smooth-joint model

The calibration of the smooth-joint (SJ) model involves conducting normal deformability and direct shear tests on planar rock joints and comparing the numerical results with experimental counterparts. According to Bahaaddini et al. (2013), the normal stiffness (k_n^{sj}) of the SJ model can be calibrated against the normal deformability test; and the shear stiffness (k_s^{sj}) and friction coefficient (μ^{sj}) of the SJ model can be calibrated against the laboratory observations of direct shear test. We used the laboratory data obtained by Oh et al. (2017) for calibrating the SJ model, and the details of the calibration procedure are provided in our previous research (Saadat and Taheri 2019b). Figure 5a illustrates the comparison between DEM simulations and laboratory results of normal deformability test. Figure 5b shows the results of numerical direct shear tests carried out on planar rock joint under various normal stress magnitudes. The plots of the corresponding peak shear stresses against the normal stress magnitudes are illustrated in Fig. 5c, and a macroscopic friction angle of 41° (friction coefficient of 0.86) was resulted which is very close to the experimental counterpart (i.e. friction coefficient of 0.9) (Oh et al. 2017). The micro-mechanical

Table 1 The calibrated micro-mechanical properties (Saadat and Taheri 2019b)

E^0 (GPa)	k^*	C^0 (MPa)	κ (m^{-1})	μ	β
9.2	1.82	23.2	2.5×10^6	0.58	0.2

Table 2 The macroscopic properties of numerical and experimental specimens (Saadat and Taheri 2019b)

	UCS (MPa)	*E* (GPa)	
Lab test (Oh et al. 2017)	46.3	14.9	0.2
Numerical modelling	46.1	14.8	0.2

properties obtained during calibration of the SJ model are given in Table 3.

Validation

The ability of the proposed cohesive DEM framework in reproducing the macroscopic shear behaviour of rock joints (i.e. dilative response and asperity degradation) was assessed. We demonstrated the details of the validation process in our previous research (Saadat and Taheri 2019b), and we briefly introduce the results here. The experimental observations of Oh et al. (2017) were used for validation purpose. To do so, we generated DEM specimens containing idealised rock joints with asperity angle of 20° and 30°. Then, we conducted a series of direct shear tests under CNL condition and compared the results with the experimental data to ensure that the calibrated DEM model is able to mimic the shear behaviour of physical specimens. Figure 6 illustrates the shear stress-displacement and normal-shear displacement curves obtained from numerical simulations. The comparison between asperity degradation of numerical specimens and experimental tests is shown in Fig. 7, and the comparison between macroscopic dilation response of the numerical specimens and laboratory counterparts is illustrated in Fig. 8.

DEM modelling results under CNS condition

It has been repeatedly reported in the previous laboratory investigations (Asadi et al. 2013; Indraratna et al. 1998, 1999; Indraratna et al. 2015; Park et al. 2013) that the surface roughness and the boundary condition (CNL and CNS) play a key role in the shear behaviour of rock joints. In this study, numerical specimens with idealised saw-tooth asperities and natural rock joint profiles were generated and tested under both CNL and CNS conditions. The numerical set-up under CNS boundary condition is illustrated in Fig. 9. Under CNS condition the increment of normal stress is expressed as:

$$d\sigma_n = k^{cns} \times d\delta_n \tag{16}$$

where k^{cns} is the constant normal stiffness at an external boundary and $d\delta_n$ is the increment of normal displacement (Indraratna et al. 2015). We adopted the servo-controlled mechanism developed by Itasca (2016) to control normal load on the top wall. As suggested by Bahaaddini et al. (2013), we calculated the shear displacement of the top-left wall to determine the shear displacement of the DEM model. In the CNS numerical models, the displacement of the top wall in the normal direction was measured at each time-step to produce the normal displacement of the rock joint. The reaction force induced on the top wall was also measured and divided by the length of rock joints to calculate the normal stress. In order to implement CNS condition in PFC 2D, the following steps were taken:

1. A relatively small velocity was applied on the top wall, and the model was solved to reach to an equilibrium. The target normal stress must be assigned at this stage. The servo-controlled mechanism was used and when the target normal stress was achieved the next steps were followed.
2. Horizontal velocity of 0.01 m/s was applied on the top left wall to simulate the shearing procedure. The increment of normal displacement was measured at each step and based on Eq. 16 the increment of normal stress was calculated. Before entering the next time step (t^{i+1}), the applied normal stress was modified by adding the increment of normal stress to the target normal stress.

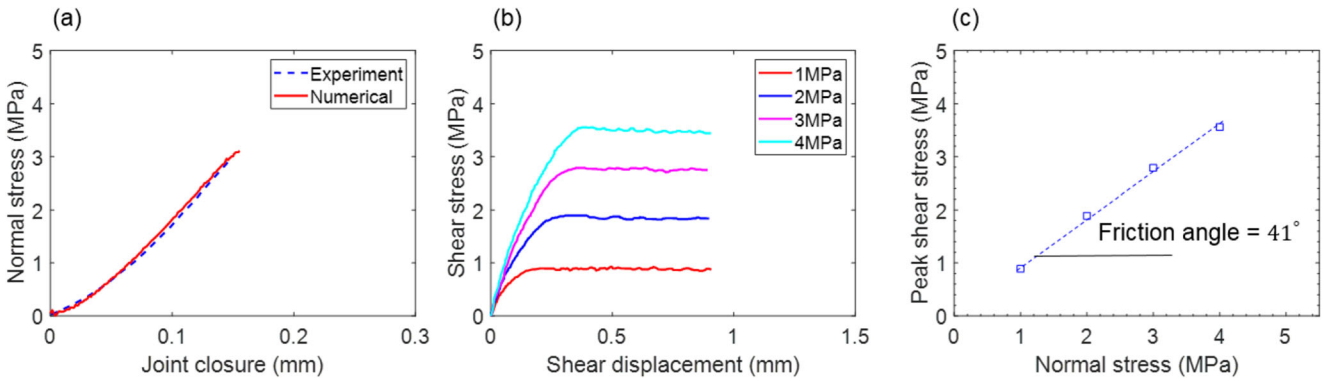

Fig. 5 The results of the smooth-joint model calibration (Saadat and Taheri 2019b). (a) Numerical and experimental normal deformability test; (b) numerical direct shear test under various constant normal stresses; (c) the friction angle of the rock joint obtained from the numerical tests

Table 3 The calibrated micro-mechanical parameters of the smooth-joint model (Saadat and Taheri 2019b)

k_n^{sj} (GPa/m)	k_s^{sj} (GPa/m)	μ^{sj}
480	55	0.9

3. The shearing procedure was continued with the updated value of applied normal stress. In order to verify the accuracy of CNS algorithm performance, the measured and calculated normal stresses were constantly compared.

In Fig. 9 the numerical simulation set-up and boundary condition required for conducting a direct shear test on rock joints is illustrated. Under CNL condition a constant normal load is required to be applied on the top plate (Figure 9a), whereas under CNS condition the normal stress increases with an increase in the normal displacement (Fig. 9b). An example of normal displacement and applied normal stress as a function of numerical time steps under CNS condition is illustrated in Fig. 9c. The initial normal stress is 0.5 MPa and the stiffness is 1.5 GPa/m. You can see that the above algorithm was successful in applying the calculated normal stress during the direct shear test (Fig. 9c).

In the following sub-sections the results of direct shear tests carried out on saw-tooth, and natural rock joints are provided, and different shear mechanisms observed in each rock joint are discussed.

Numerical direct shear test of saw-tooth asperities under CNS condition

In the previous section, a series of CNL direct shear tests on saw-tooth joints under a range of normal stress magnitude were conducted and the simulation outcomes were compared with the experimental counterparts. In this section, the influence of CNS condition on the shear behaviour of saw-tooth asperities is investigated. Specifically, the asperity degradation is visualised by monitoring the evolution of DEM micro-cracks. Notice that, for CNS testing, the identical sample size and the same calibrated micro-parameters were adopted. In total, eighteen CNS direct shear tests were carried out on saw-tooth asperities, and for each initial normal stress, σ_n^0, magnitude, three different values of k^{cns}: 0.5, 1, and 1.5 GPa/m were considered. The simulated shear stress and normal displacement as a function of shear displacement for saw-tooth asperities are shown in Fig. 10. The asperity damage of numerical specimens after 2.5 mm of shear displacement for both asperity angle, i, values of 20° and 30° is illustrated in Fig. 11. In order to facilitate the comparison of numerical results, in each graph, k^{cns} was kept constant and asperity base angle as well as the σ_n^0 were varied.

At low σ_n^0, by increasing the constant stiffness, the shear mechanism of specimens with $i = 20°$ was gradually transferred from asperity sliding to a combination of asperity sliding and wear. You can see this in both shear stress-displacement graphs (Fig. 10), and macroscopic cracking behaviour of the specimens (Fig. 11). In contrast, at low initial normal stress, specimens with $i = 30°$ showed a remarkable shift from asperity sliding to asperity shear-off and severe asperity degradation (Fig. 11; $\sigma_n^0 = 0.5MPa$ and $i = 30°$). Increase of constant stiffness (k^{cns}) under σ_n^0 of 2 and 4 MPa

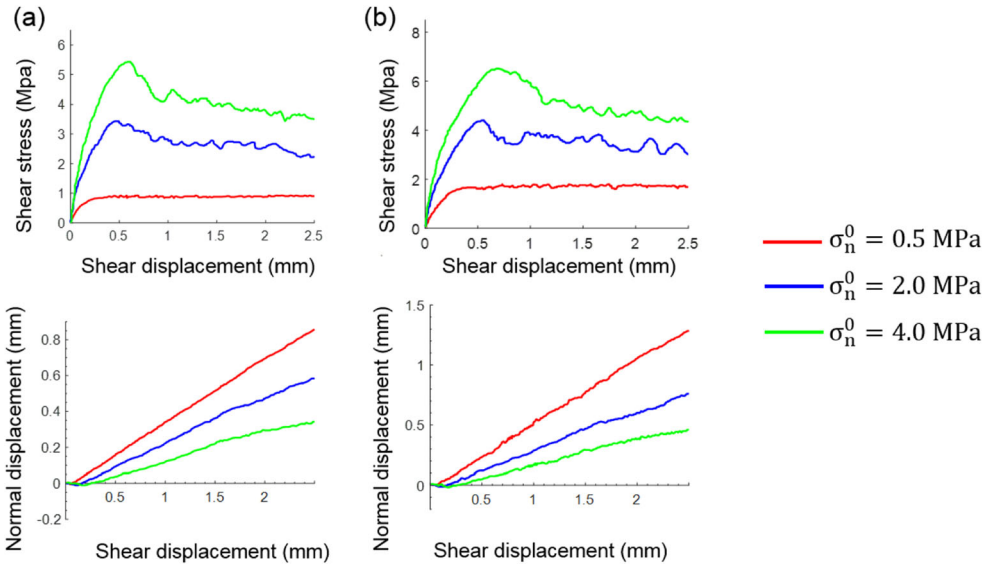

Fig. 6 The numerical shear behaviour of idealised saw-toothed rock joints under various normal stress magnitudes: (a) $i = 20°$, and (b) $i = 30°$ (modified from Saadat and Taheri (2019b))

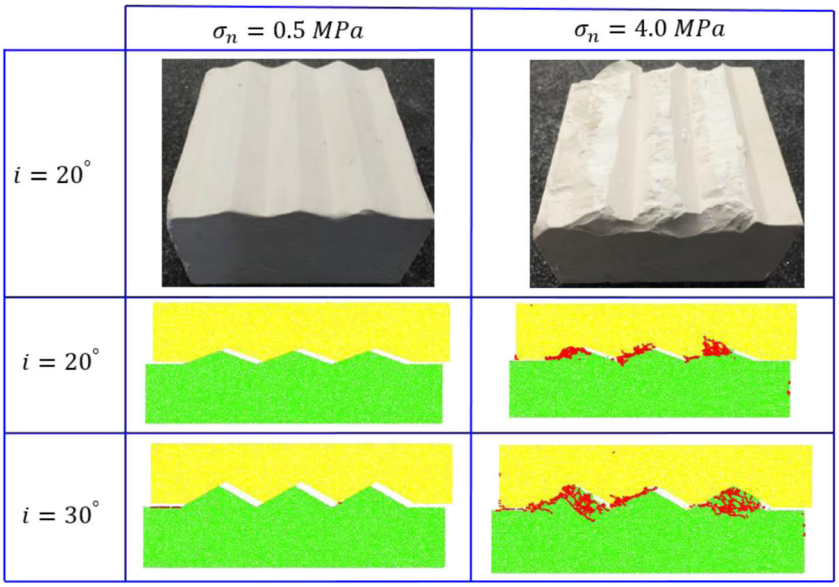

Fig. 7 The asperity damage response obtained from numerical simulations under low and high confinement. The experimental tests carried out by Oh et al. (Oh et al. 2017) and the numerical results are modified from Saadat and Taheri (2019b)

results in an increase in the peak shear strength when the base angle is equal to 30 °. This influence, however, found to be negligible when the base angle is equal to 20° (Fig. 10). This may be attributed to the fact that rock joints with steeper asperity angle require more shear force to mobilise the asperities resulting in a considerable peak shear stress of rock joints. The results also revealed that at greater levels of σ_n^0 with low k^{cns}, the increase in the shear resistance of rock joints was less significant, as a result of severe asperity damage. In contrast, at low confining stress level, the influence of CNS condition on the macroscopic shear response of the joints was much more pronounced especially when $i = 30°$. These results reveal that to design underground structures, CNS condition needs to be taken into account when dealing with low initial normal stress magnitudes (i.e. $^{\sigma_n}/_{\sigma_c} \leq 1\%$). This conclusion will be further discussed later on.

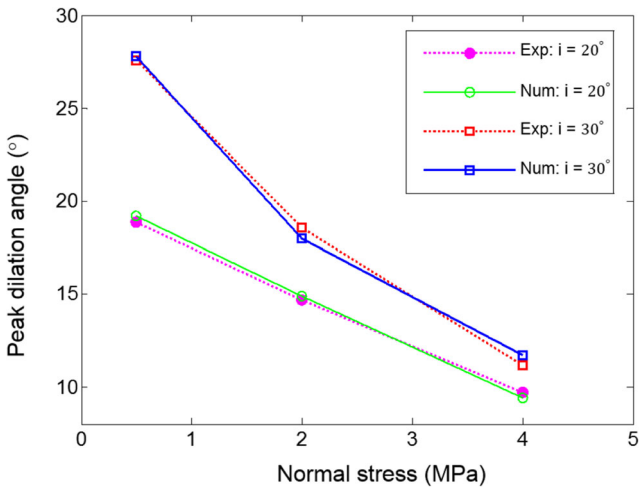

Fig. 8 Numerical and experimental comparison for peak dilation angle of idealised rock joints under various normal stress magnitudes. The experimental tests carried out by Oh et al. (Oh et al. 2017). The numerical data are from Saadat and Taheri (2019b)

Monitoring the normal displacement of the rock joints (Fig. 10) showed that the dilation of numerical specimens with i of 30° was higher than $i = 20°$ in all the cases. For both specimens, the value of normal displacement decreased with an increase in the constant stiffness, which is attributed to the relative increase of applied normal stress rate. In the specimens with 20° of asperity angle, the joint returned almost the same normal displacement response under different initial normal stress magnitudes and this behaviour was more conspicuous for a specimen with 1.5 GPa/m of constant normal stiffness. It can also be seen that at 1.5 GPa/m of constant stiffness, in the specimens with $i = 30°$, after approximately 1.5 mm of shear displacement, the rock joint maintained its normal displacement at a level close to 0.4 mm. This exhibition of frictional sliding response was due to considerable asperity degradation caused by a higher degree of σ_n^0.

Numerical direct shear test of natural rock joint profiles under CNS condition

Three different natural rock joint profiles with joint roughness coefficient (JRC) values of 4.6 (smooth), 10.2 (rough), and 17.5 (very rough) obtained from joints in Hawkesbury sandstone were digitised and imported into PFC 2D. Figure 12 illustrates these natural rock joints. The average values of JRC for each profile were previously determined by Bahaaddini (Bahaaddini 2014). We digitised the rock joint interfaces in AutoCAD software and imported the files into PFC2D to construct the geometry of rock joint. We developed a series of FISH functions to group the DEM particles into

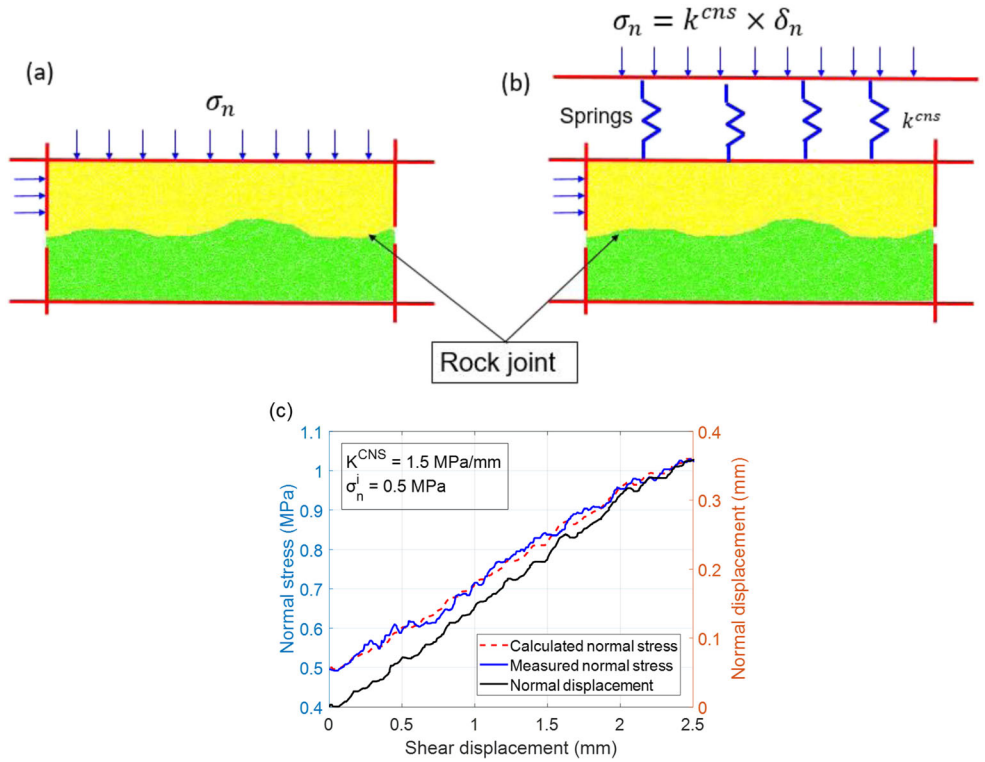

Fig. 9 Direct shear test simulation of rock joint under different loading conditions. (a) CNL condition, (b) CNS condition, (c) normal displacement versus mechanical time step, (b) calculated and applied normal stress under CNS condition during the shearing process

upper and lower blocks. Hereafter, the numerical specimens with JRC values of 4.6, 10.2, and 17.5 are called JP1, JP2, and JP3, respectively. k^{cns} of 0.5, 1, and 1.5 GPa/m were considered in numerical CNS direct shear tests to examine the influence of CNS condition on the macroscopic behaviour of rock joints.

In Fig. 13, CNL and CNS direct shear test results of JP2 (k^{cns} = 1 GPa/m) under different initial normal stress magnitudes are presented as representative results. The results show that the slope of linear-elastic portion of the shear stress-displacement curves (Fig. 13a) for each CNS increases with an increase in the initial normal stress magnitude. All the

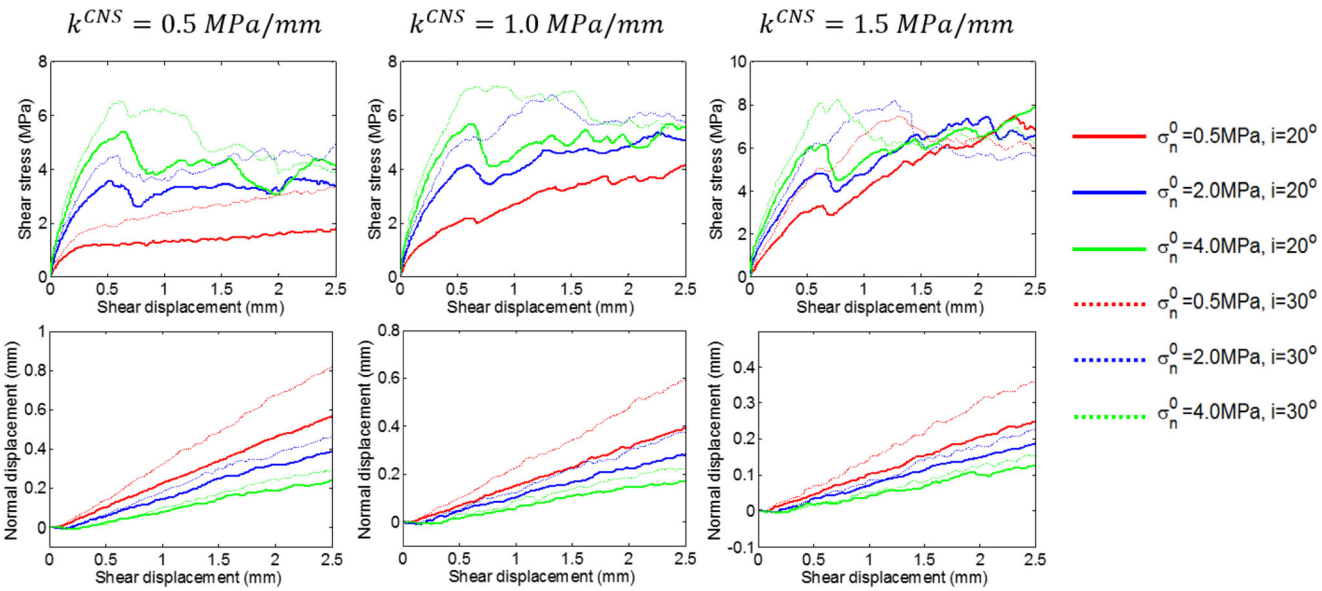

Fig. 10 Numerical direct shear test results of idealised rock joints under CNS condition

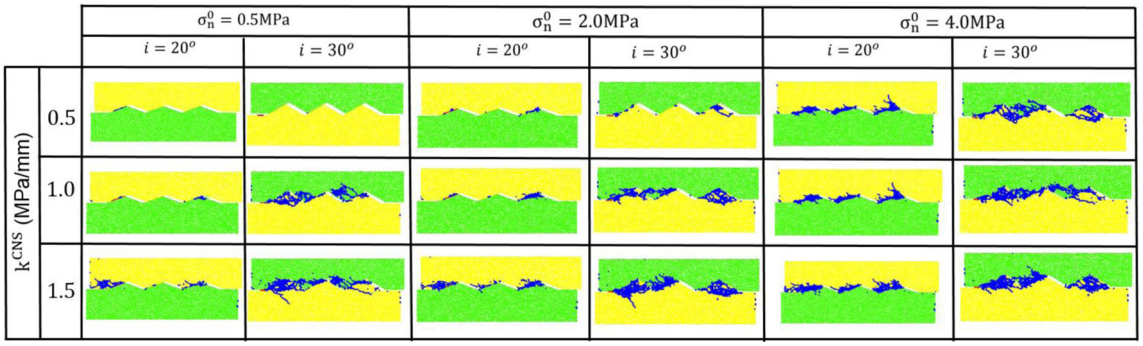

Fig. 11 Numerical asperity damage of idealised rock joints under CNS condition

numerical specimens exhibited a slight strain-hardening behaviour before reaching their peak shear strength (Fig. 13a). It is important to note that the shear stress-displacement curves do not present a distinct peak shear strength for the specimen with 0.5 MPa of initial normal stress. The reason for exhibiting such behaviour is due to the progressive increment of normal stress magnitude throughout the shearing process (Indraratna et al. 2015). It can be seen that when the magnitude of initial normal stress increased, the numerical specimens returned very few hardening responses (Fig. 13a). This may be due to the transition from asperity sliding mode to asperity wear and shear-off modes that cause progressive asperity degradation in these specimens. In fact, severe bond-break in the cohesive contacts, under high initial normal stress, means that the shear resistance of the asperities is proportionately ineffective during the residual stage. We observed this mechanism by monitoring the initiation of micro-cracks during the shearing process (Fig. 13b). You can see that after a relative shear displacement of approximately 0.3 mm, the propagation rate of cohesive micro-crack experienced a significant rise in the synthetic specimens with high initial normal stress magnitude.

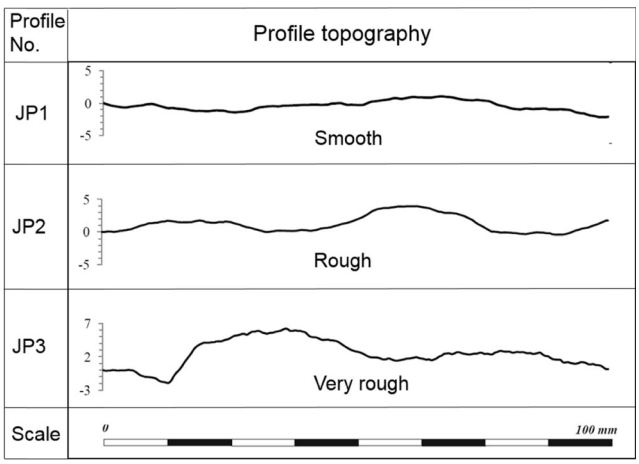

Fig. 12 Natural rock joint profiles considered in the parametric study approach. (modified from (Bahaaddini 2014))

The dilation response of the numerical specimens is illustrated in Fig. 13c. You can observe that the dilation of rock joint was strongly influenced by the magnitude of the initial normal stress. As the initial normal stress increased, the normal displacement of the rock joint reduced significantly that was the result of the transition from asperity sliding mode to asperity wear and shear-off modes.

The asperity degradation pattern that was the results of initiation and coalescence of micro-cracks was monitored for both CNL and CNS experiments, and the results are illustrated for JP2 in Fig. 13 as representative results. Under CNL condition, by increasing the magnitude of normal stress, the number of micro-cracks significantly increased, especially around the critical asperities. You can see from Fig. 13c and Fig. 14 that the CNS specimens tended to produce more micro-cracks. The results show that severe asperity damage occurred at high normal stress magnitudes, while a combination of slight asperity wear-off, as well as sliding mode, controlled the shear mechanism of the joint at low confining pressure.

The influence of joint roughness on the shear behaviour of rock joints under CNS condition is illustrated in Fig. 15. The macroscopic asperity damage responses of the specimens are illustrated in Fig. 16. The initial normal stress and k^{cns} in all the specimens were 0.5 MPa and 1.0 GPa/m, respectively. As shown in Fig. 14a, the JP3, with the highest amount of JRC (i.e. JRC = 17.5), shows a higher peak shear strength. It can be observed that JP1 and JP2 exhibit asperity sliding behaviour while JP3 during shearing demonstrates a remarkable asperity shear-off (Figs. 15a and 16). This mechanism was verified by monitoring the number of micro-crack initiated during the shearing procedure (Fig. 15b). It can be quantitatively observed that a relatively few numbers of micro-cracks propagated during shearing of JP1, whereas the number significantly increased with an increase in JRC.

Experimental observations of Yang and Chiang (Yang and Chiang 2000) and Li et al. (Li et al. 2016b) showed that asperities mainly controlled the shear resistance and dilative response of rock joints with higher inclination angle. Li et al. (Li et al. 2016b) defined critical asperity angle as the

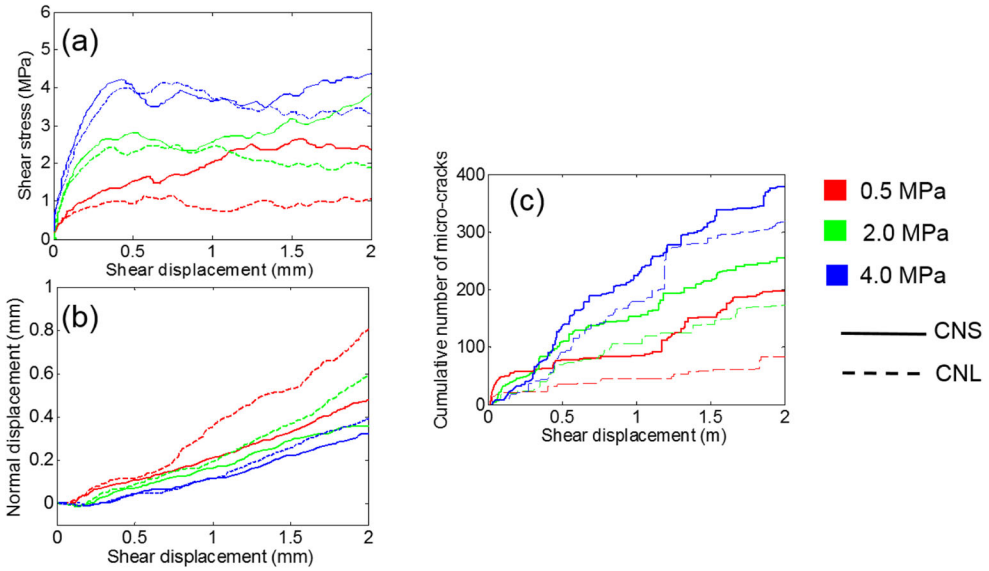

Fig. 13 Numerical direct shear test results of natural rock joint profile (JP2) under CNL and CNS (k^{cns} = 1 GPa/m) conditions: (a) and (b) shear stress-displacement and normal-shear displacement curves, respectively; (c) cumulative number of micro-cracks developed in the rock joint profile

steepest waviness facing the shear direction. The PFC-DEM approach allowed us to visually observe the location of critical asperities where the density of micro-cracks is relatively high due to asperity failure (Fig. 16). It can be seen from Fig. 16 that JP1 experienced a sliding mode with minor micro-cracks propagated on the joint surface, while higher JRC values returned severe asperity wear (JP2), and asperity shear-off (JP3). Previous numerical results (Fig. 10) also showed that an idealised rock joint with higher asperity angle exhibit the highest value of normal stress during shearing (both under CNL and CNS conditions). We can confirm from Fig. 15b that the rock joints with higher value of JRC (or higher critical asperity angle) displayed a greater dilation during the shearing process (Fig. 15b). Figure 15c illustrates the cumulative number of micro-cracks during shear process. It can be seen that very rough rock joint profile (JP3) exhibited severe asperity damage. Its high number of micro-cracks also indicates this behaviour compared with other profiles.

Numerical shear behaviour of bolted rock joints under CNS condition

In order to investigate the influence of CNS condition on the overall shear performance of bolted rock joints using the new cohesive model, a series of numerical CNS direct shear tests were carried out on different rock joint profiles: JP1, JP2, and JP3. To avoid making this paper overly long, a simplification is made by only considering single values for normal stress and k^{cns}. Notice that the performance of fully grouted rock bolts can only be simulated in 3D. However, in 2D a section

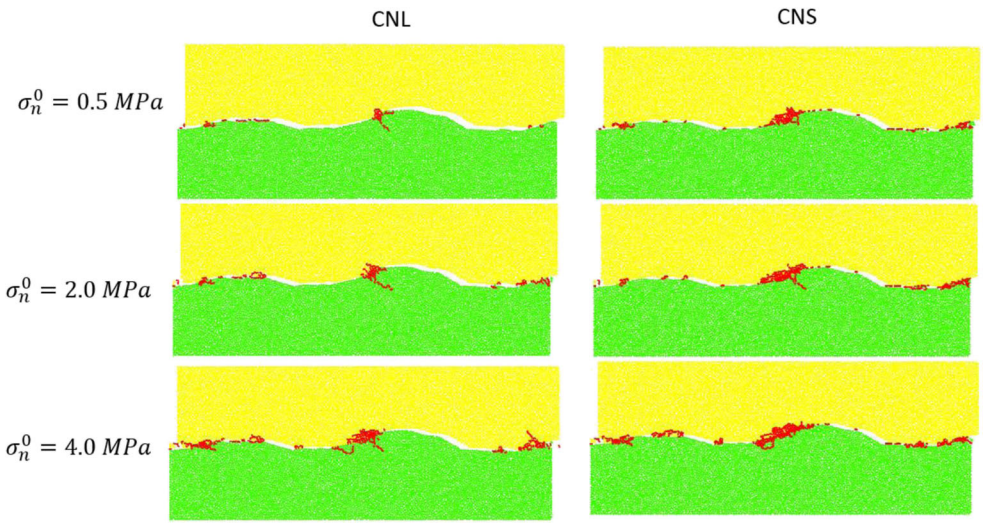

Fig. 14 Numerical asperity degradation for natural rock joint (JP2) under CNS (k^{cns} = 1 GPa/m) condition

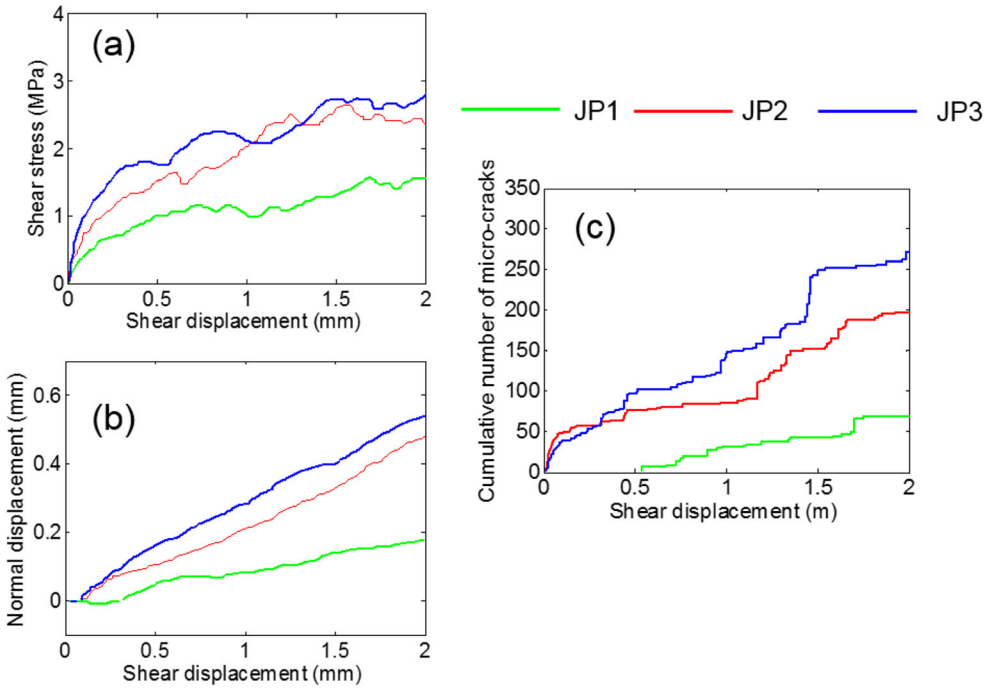

Fig. 15 Numerical direct shear test results carried out on three different natural rock joints with various JRC values under CNS (k^{cns} = 1 GPa/m) condition: (a) and (b) shear stress-displacement and normal-shear displacement curves, respectively; (c) the cumulative number of micro-cracks developed in the rock joint profile

of the 3D model can be simulated (as rock panel) to evaluate the mechanical behaviour of bolted rock joints. We compared the simulation results with those obtained for unbolted rock joints under CNL and CNS conditions. The rock bolts were considered to be fully grouted. Furthermore, it was assumed that the rock bolts only deform elastically along the shear direction without producing any rupture behaviour. This assumption was also considered in the experimental investigations of Wu et al. (2018) and Chen et al. (2018) to investigate the influence of surface roughness. We assumed no damage on rock bolt element and only the grout material fails during the test. Thus, a high value of bond strength was sufficient to prevent bond failure in the rock bolt element. We selected the micro-mechanical properties of rock bolt based on the previous literature (Shang et al. 2018a). We also adopted the same approach in our previous rock bolt investigation (Saadat and Taheri 2019b). Notice that no particular rock bolt was considered in the current study as the aim was investigating the influence of boundary condition and surface roughness on the shear behaviour of reinforced joints. Accordingly, it is justified to consider the rock bolt element without experiencing failure during shear testing.

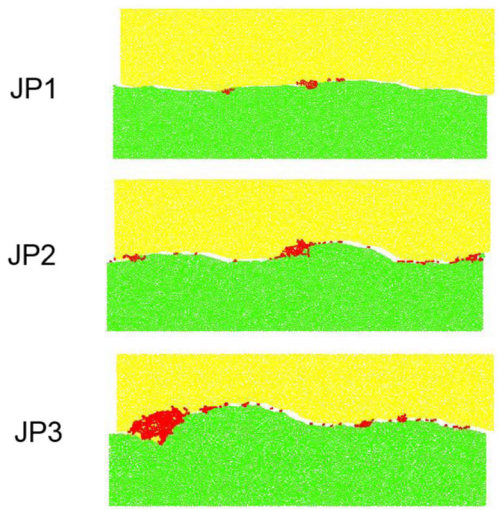

Fig. 16 Numerical asperity damage observed in various natural rock joints under CNS (k^{cns} = 1 *G*Pa/m) condition

The cohesive model was used as the constitutive model of the grout material. The micro-mechanical parameters of the grout were calibrated against the properties of grouting material experimentally obtained by (Kılıc et al. 2002). The calibrated micro-mechanical parameters, as well as macroscopic properties of experimental and numerical specimens, are given in Table 4. The thickness of grout material around the rock bolt was 2 mm, and the diameter of the rock bolt was 4 mm. In order to generate the numerical specimens for the CNL and CNS direct shear tests, the particles were grouped in three different categories: rock, rock bolt, and grout. The micro-mechanical parameters for each group were assigned according to their contact group. Apart from rock joint interface particles, two more interfaces were generated in bolt models, namely bolt-grout and grout-rock interfaces. The micro-

Table 4 The calibrated micro-mechanical parameters and macroscopic parameters of the grout material

Micro-mechanical parameters					
E^0 (GPa)	k^*	C^0 (MPa)	κ (m^{-1})	μ	β
4.2	1.45	18.0	14.0×10^6	0.50	0.22
Macroscopic parameters					
	E (GPa)	UCS (MPa)			
Experiment (Kılıc et al. 2002)	7.4	32.0	–		
Numerical	7.3	32.0	0.18		

parameters calibrated for grout material was assigned to the contacts forming theses interfaces. The smooth-joint model with previously calibrated micro-parameters was adopted to simulate the shear behaviour of rock joints. The CNS condition was applied to the numerical specimens based on the procedure described before.

The shear stress and normal displacement as a function of the shear displacement of three numerical specimens with different roughness profiles is illustrated in Fig. 17. The failure state of the bolted and unbolted specimens at the final stage of the shearing procedure is depicted in Fig. 18. It can be observed that, for all numerical specimens, the peak shear strength of the rock joint under CNS condition was higher than those under CNL condition. The results also indicate that the JRC values highly influenced the shear behaviour of rock joints. A closer assessment of the results presented in Fig. 17 indicates that for JP3, the increase in the value of shear resistance was not highly significant, especially under CNL condition. This was attributed to considerable asperity damage because of greater JRC value. For bolted rock joints during the post-peak stage, significant volatility was observed in the shear stress-displacement curves that were the results of an increase in the resistance of the rock joints against shearing, generated by the rock bolt.

The results presented in Fig. 17 show that the shear strengths of rock joints with low JRC (JP1) and medium (JP2) JRC values exhibit considerable sensitivity to rock bolt installation as well as CNS condition. In contrast, at high JRC values in bolted condition, severe asperity degradation (due to higher roughness) under CNS condition prevented the rock joints from returning a considerably higher peak shear stress (Fig. 18). Consequently, the CNS results, in terms of elastic response and peak shear stress, were not highly comparable to those of CNL. During the post-peak stage, however, the CNL specimen maintained the shear resistance while CNS specimen returned a hardening behaviour as a result of an increase in the applied normal stress. It should be noted that in JP2 and JP3 specimens, as a result of rock bolt installation, fractures

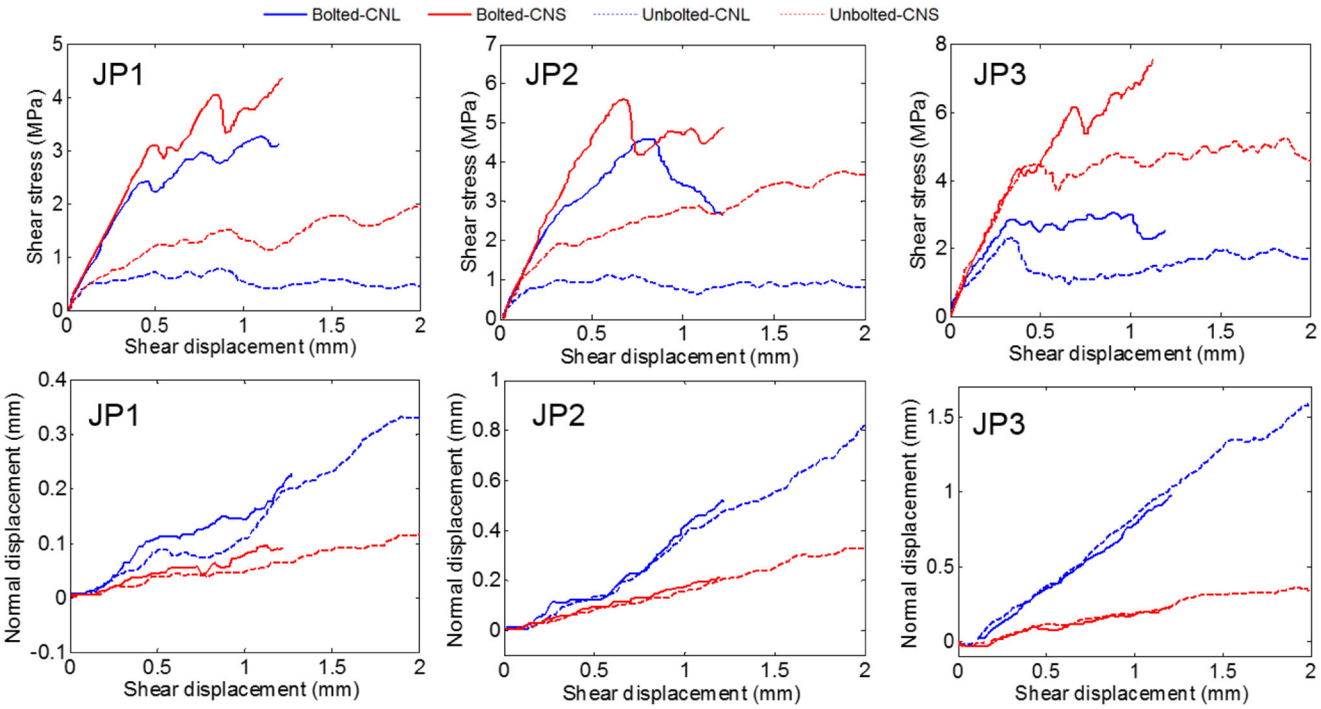

Fig. 17 The direct shear test results of unbolted and bolted rock joints under CNL and CNS (k^{cns} = 1 GPa/m) conditions

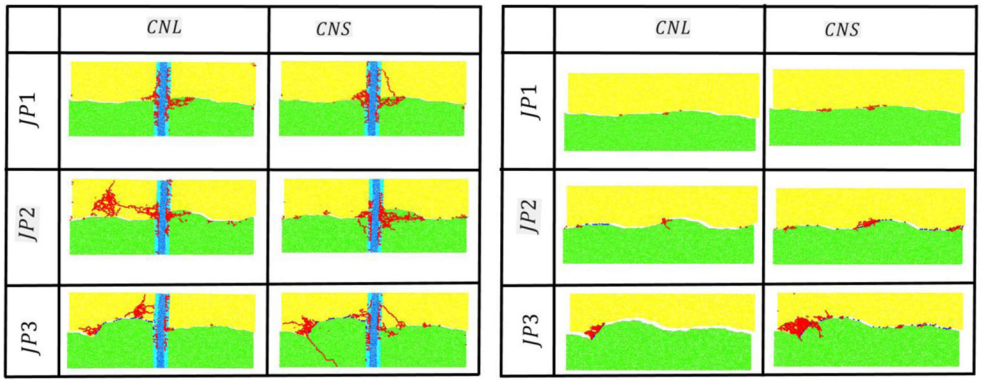

Fig. 18 The asperity damage of unbolted and bolted natural rock joint profiles under CNL and CNS (k^{cns} = 1 GPa/m) conditions

were developed in some areas of the specimen (particularly the bottom rock block was fractured for JP3-CNS, Fig. 18). It is desirable in a direct shear test of unbolted rock joints to have only asperity degradation along the surface of rock joints. However, according to previous studies related to rock bolt direct shear testing, such fracturing of the specimens is inevitable (Chen et al. 2018).

The normal-shear displacement curves revealed that under CNS condition, both bolted and unbolted specimens produced the same dilation behaviour. Under CNL condition, however, bolted specimens with JP1 and JP2 showed significantly higher normal displacement. By increasing the roughness of the profiles to JP3, the normal displacement of the bolted and unbolted rock joints were approximately identical under both CNL and CNS conditions. It is believed that for JP1 and JP2, the high resistance of the joint against shearing due to installation of rock bolt caused the top block to move upward during shearing process, leading to a relatively higher value of normal displacement. In comparison, when the roughness of the rock joint was high (JP3), the severe asperity damage in the rock joint allowed the specimen to move down even under CNL condition. As a result, the JP3 profile returned identical normal displacement under both CNL and CNS conditions.

Conclusion

In this study, a cohesive contact model implemented in DEM code was employed to numerically study the shear behaviour of bolted and unbolted rock joints under CNL and CNS conditions. The numerical results were compared with the laboratory observations of rock joint asperity degradation. This was to ensure that the model worked properly and was able to mimic the mechanical behaviour of rock joints. After validating the model, we performed a parametric study on rock joint characteristics (JRC) and boundary condition (CNL and CNS) to investigate more the shear behaviour of rock joints. A parametric study was carried on bolted rock joints to assess the shear behaviour of rock joints reinforced by fully grouted rock bolts. In the present study, the effect of asperity angle, surface roughness, and boundary condition (i.e. CNL and CNS condition) on shear behaviour of both bolted and unbolted rock joints were investigated. The following concluding remarks can be drawn:

- For idealised saw-tooth asperities, when the initial normal stress was low, specimens with steeper asperity angle showed a higher degree of asperity damage by increasing the constant stiffness. The CNS numerical results also showed that at low asperity angle the shear resistance of the rock joint could not be enhanced, while the steeper asperities experienced a considerable improvement in peak shear stress. The normal displacement of steeper asperities was higher than low asperity angle specimens. Under the CNS condition, the normal-shear displacement curves for higher asperity angles showed more distinct differences than low asperity angle.
- Apart from the idealised rock joint, three natural rock joint profiles representing smooth, rough, and very rough rock joints were tested. The CNS numerical results revealed that the asperity degradation profoundly influenced the shear behaviour of specimens including natural rock joint profiles, the extent of which increased with increasing the value of JRC and initial applied normal stress. The shear stress was profoundly influenced by the CNS condition at low initial confining pressure, while the negligible effect was observed at the medium and high level of initial normal stress. This is mainly because of the serious asperity damage under high confining pressure, which prevents the CNS condition to affect the rock joint's shear and dilation responses. By increasing the roughness, the shear mechanism transformed from asperity sliding to asperity shear-off and significant asperity damage. Compared with lower roughness values, the joint with the highest JRC showed the highest dilation.
- A rock bolting system was also generated to investigate the shear mechanism of bolted rock joints containing natural profiles. It was observed that rock bolt installation

significantly improved the peak shear strength of the rock joints under both CNL and CNS conditions. When the asperity is damaged significantly under CNS condition, the normal displacements of the both bolted and unbolted rock joints were identical. The peak shear strength of bolted rock joint under CNS condition was higher than those under CNL condition. Under CNS condition, the specimens with the highest JRC value returned approximately an identical peak shear strength for the both bolted and unbolted rock joints that were the result of remarkable asperity degradation of the highly rough interface.

Acknowledgements We appreciate the valuable comments from Giang D. Nguyen (University of Adelaide). The first author thanks Mr. Sacha Emam from Itasca Consulting group for his invaluable help and comments during implementation and verification of the model in PFC software.

Compliance with ethical standards

Conflict of interest The authors declare that they have no conflict of interest.

References

Asadi MS, Rasouli V, Barla G (2012) A bonded particle model simulation of shear strength and asperity degradation for rough rock fractures. Rock Mech Rock Eng 45:649–675. https://doi.org/10.1007/s00603-012-0231-4

Asadi MS, Rasouli V, Barla G (2013) A laboratory shear cell used for simulation of shear strength and asperity degradation of rough rock fractures. Rock Mech Rock Eng 46:683–699. https://doi.org/10.1007/s00603-012-0322-2

Bahaaddini M (2014). Numerical study of the mechanical behaviour of rock joints and non-persistent jointed rock masses. Ph.D. thesis, The University of New South Wales, Sydney, Australia

Bahaaddini M, Sharrock G, Hebblewhite B (2013) Numerical direct shear tests to model the shear behaviour of rock joints. Comput Geotech 51:101–115

Bahaaddini M, Hagan PC, Mitra R, Hebblewhite BK (2015) Parametric study of smooth joint parameters on the shear behaviour of rock joints. Rock Mech Rock Eng 48:923–940. https://doi.org/10.1007/s00603-014-0641-6

Bewick RP, Kaiser PK, Bawden WF (2014) Shear rupture under constant normal stiffness boundary conditions. Tectonophysics 634:76–90. https://doi.org/10.1016/j.tecto.2014.07.016

Bi Y, He S, Du Y, Sun X, Li X (2019) Effects of the configuration of a baffle–avalanche wall system on rock avalanches in Tibet Zhangmu: discrete element analysis. Bull Eng Geol Environ 78:2267–2282. https://doi.org/10.1007/s10064-018-1284-8

Cao RH, Cao P, Lin H, Ma GW, Fan X, Xiong XG (2018a) Mechanical behavior of an opening in a jointed rock-like specimen under uniaxial loading: experimental studies and particle mechanics approach. Arch Civ Mech Eng 18:198–214. https://doi.org/10.1016/j.acme.2017.06.010

Cao RH, Cao P, Lin H, Ma GW, Zhang CY, Jiang C (2018b) Failure characteristics of jointed rock-like material containing multi-joints under a compressive-shear test: experimental and numerical analyses. Arch Civ Mech Eng 18:784–798. https://doi.org/10.1016/j.acme.2017.12.003

Chen Y, Li C (2015a) Influences of loading condition and rock strength to the performance of rock bolts. Geotech Test J 38:208–218. https://doi.org/10.1520/GTJ20140033

Chen Y, Li CC (2015b) Performance of fully encapsulated rebar bolts and D-bolts under combined pull-and-shear loading. Tunn Undergr Space Technol 45:99–106. https://doi.org/10.1016/j.tust.2014.09.008

Chen N, Zhang X, Jiang Q, Feng X, Wei W, Yi B (2018) Shear behavior of rough rock joints reinforced by bolts. Int J Geomech 18:04017130. https://doi.org/10.1061/(ASCE)GM.1943-5622.0001048

Dey A (2001). Shear behaviour of fully grouted bolts under constant normal stiffness condition. Ph.D. thesis, University of Wollongong, NSW, Australia

Ghadimi M, Shahriar K, Jalalifar H (2015) A new analytical solution for the displacement of fully grouted rock bolt in rock joints and experimental and numerical verifications. Tunn Undergr Space Technol 50:143–151. https://doi.org/10.1016/j.tust.2015.07.014

Ghazvinian A, Sarfarazi V, Schubert W, Blumel M (2012) A study of the failure mechanism of planar non-persistent open joints using PFC2D. Rock Mech Rock Eng 45:677–693. https://doi.org/10.1007/s00603-012-0233-2

Grasselli G (2005) 3D behaviour of bolted rock joints: experimental and numerical study. Int J Rock Mech Min Sci 42:13–24. https://doi.org/10.1016/j.ijrmms.2004.06.003

Gutiérrez-Ch JG, Senent S, Melentijevic S, Jimenez R (2018) Distinct element method simulations of rock-concrete interfaces under different boundary conditions. Eng Geol 240:123–139. https://doi.org/10.1016/j.enggeo.2018.04.017

Hofmann H, Babadagli T, Yoon JS, Zang A, Zimmermann G (2015) A grain based modeling study of mineralogical factors affecting strength, elastic behavior and micro fracture development during compression tests in granites. Eng Fract Mech 147:261–275. https://doi.org/10.1016/j.engfracmech.2015.09.008

Indraratna B, Welideniya H (2003) Shear behaviour of graphite infilled joints based on constant normal stiffness (CNS) test conditions. Paper presented at the 10th ISRM congress, Sandton, South Africa

Indraratna B, Haque A, Aziz N (1998) Laboratory modelling of shear behaviour of soft joints under constant normal stiffness conditions. Geotech Geol Eng 16:17–44. https://doi.org/10.1023/a:1008880112926

Indraratna B, Haque A, Aziz N (1999) Shear behaviour of idealized infilled joints under constant normal stiffness. Géotechnique 49:331–355. https://doi.org/10.1680/geot.1999.49.3.331

Indraratna B, Thirukumaran S, Brown ET, Zhu S-P (2015) Modelling the shear behaviour of rock joints with asperity damage under constant normal stiffness. Rock Mech Rock Eng 48:179–195. https://doi.org/10.1007/s00603-014-0556-2

Itasca. (2016) PFC manual, version 5.0, Minneapolis

Jalalifar H, Aziz N (2010) Experimental and 3D numerical simulation of reinforced shear joints. Rock Mech Rock Eng 43:95–103. https://doi.org/10.1007/s00603-009-0031-7

Jalalifar H, Aziz N, Hadi M (2006) The effect of surface profile, rock strength and pretension load on bending behaviour of fully grouted bolts. Geotech Geol Eng 24:1203–1227. https://doi.org/10.1007/s10706-005-1340-6

Kazerani T, Yang Z, Zhao J (2012) A discrete element model for predicting shear strength and degradation of rock joint by using compressive and tensile test data. Rock Mech Rock Eng 45:695–709

Kılıc A, Yasar E, Celik AG (2002) Effect of grout properties on the pull-out load capacity of fully grouted rock bolt. Tunn Undergr Space Technol 17:355–362. https://doi.org/10.1016/S0886-7798(02)00038-X

Le LA, Nguyen GD, Bui HH, Sheikh AH, Kotousov A, Khanna A (2017) Modelling jointed rock mass as a continuum with an embedded

cohesive-frictional model. Eng Geol 228:107–120. https://doi.org/10.1016/j.enggeo.2017.07.011

Le LA, Nguyen GD, Bui HH, Sheikh AH, Kotousov A, Khanna A. (2018) Localised failure mechanism as the basis for constitutive modelling of geomaterials. Int J Eng Sci 133:284–310

Li L, Hagan PC, Saydam S, Hebblewhite B, Li Y (2016a) Parametric study of Rockbolt shear behaviour by double shear test. Rock Mech Rock Eng 49:4787–4797. https://doi.org/10.1007/s00603-016-1063-4

Li Y, Oh J, Mitra R, Hebblewhite B (2016b) A constitutive model for a laboratory rock joint with multi-scale asperity degradation. Comput Geotech 72:143–151. https://doi.org/10.1016/j.compgeo.2015.10.008

Li Y, Zhou H, Zhang L, Zhu W, Li S, Liu J (2016c) Experimental and numerical investigations on mechanical property and reinforcement effect of bolted jointed rock mass. Constr Build Mater 126:843–856. https://doi.org/10.1016/j.conbuildmat.2016.09.100

Lin H, Xiong Z, Liu T, Cao R, Cao P (2014) Numerical simulations of the effect of bolt inclination on the shear strength of rock joints. Int J Rock Mech Min Sci 66:49–56. https://doi.org/10.1016/j.ijrmms.2013.12.010

Liu J, Yang H, Wen H, Zhou X (2017) Analytical model for the load transmission law of rock bolt subjected to open and sliding joint displacements. Int J Rock Mech Min Sci 100:1–9. https://doi.org/10.1016/j.ijrmms.2017.01.018

Liu G, Cai M, Huang M (2018) Mechanical properties of brittle rock governed by micro-geometric heterogeneity. Comput Geotech. https://doi.org/10.1016/j.compgeo.2017.11.013

Marczewska I, Rojek J, Kačianauskas R (2016) Investigation of the effective elastic parameters in the discrete element model of granular material by the triaxial compression test. Arch Civ Mech Eng 16:64–75. https://doi.org/10.1016/j.acme.2015.09.010

Nguyen NHT, Bui HH, Nguyen GD, Kodikara J (2017a) A cohesive damage-plasticity model for DEM and its application for numerical investigation of soft rock fracture properties. Int J Plast 98:175–196. https://doi.org/10.1016/j.ijplas.2017.07.008

Nguyen NHT, Bui HH, Nguyen GD, Kodikara J, Arooran S, Jitsangiam P (2017b) A thermodynamics-based cohesive model for discrete element modelling of fracture in cemented materials. Int J Solids Struct 117:159–176. https://doi.org/10.1016/j.ijsolstr.2017.03.027

Oh J, Li Y, Mitra R, Canbulat I (2017) A numerical study on dilation of a saw-toothed rock joint under direct shear. Rock Mech Rock Eng 50:913–925

Park J-W, Song J-J (2009) Numerical simulation of a direct shear test on a rock joint using a bonded-particle model. Int J Rock Mech Min Sci 46:1315–1328. https://doi.org/10.1016/j.ijrmms.2009.03.007

Park J-W, Lee Y-K, Song J-J, Choi B-H (2013) A constitutive model for shear behavior of rock joints based on three-dimensional quantification of joint roughness. Rock Mech Rock Eng 46:1513–1537. https://doi.org/10.1007/s00603-012-0365-4

Potyondy D, Cundall P (2004) A bonded-particle model for rock. Int J Rock Mech Min Sci 41:1329–1364

Saadat M, Taheri A (2019a) A cohesive discrete element based approach to characterizing the shear behavior of cohesive soil and clay-infilled rock joints. Comput Geotech 114:103–109. https://doi.org/10.1016/j.compgeo.2019.103109

Saadat M, Taheri A (2019b) Effect of contributing parameters on the behaviour of a bolted rock joint subjected to combined pull-and-shear Loading: A DEM Approach. Rock Mech Rock Eng. https://doi.org/10.1007/s00603-019-01921-6

Saadat M, Taheri A (2019c) Modelling micro-cracking behaviour of pre-cracked granite using grain-based distinct element model. Rock Mech Rock Eng. https://doi.org/10.1007/s00603-019-01862-0

Saadat M, Taheri A (2019d) A numerical approach to investigate the effects of rock texture on the damage and crack propagation of a pre-cracked granite. Comput Geotech 111:89–111. https://doi.org/10.1016/j.compgeo.2019.03.009

Saadat M, Taheri A (2019e) A numerical approach to investigate the effects of rock texture on the damage and crack propagation of a pre-cracked granite. Comput Geotech (Accepted for publication). https://doi.org/10.1016/j.compgeo.2019.03.009

Saadat M, Taheri A (2020) A cohesive grain based model to simulate shear behaviour of rock joints with asperity damage in polycrystalline rock. Comput Geotech 117:103254. https://doi.org/10.1016/j.compgeo.2019.103254

Shang J, Yokota Y, Zhao Z, Dang W (2018a) DEM simulation of mortar-bolt interface behaviour subjected to shearing. Construct Build Mater 185:120–137. https://doi.org/10.1016/j.conbuildmat.2018.07.044

Shang J, Zhao Z, Hu J, Handley K (2018b) 3D particle-based DEM investigation into the shear behaviour of incipient rock joints with various geometries of rock bridges. Rock Mech Rock Eng. https://doi.org/10.1007/s00603-018-1531-0

Shang J, Zhao Z, Ma S (2018c) On the shear failure of incipient rock discontinuities under CNL and CNS boundary conditions: insights from DEM modelling. Eng Geol 234:153–166. https://doi.org/10.1016/j.enggeo.2018.01.012

Shrivastava A, Rao K (2018) Physical modeling of shear behavior of infilled rock joints under CNL and CNS boundary conditions. Rock Mech Rock Eng 51:101–118

Spang K, Egger P (1990) Action of fully-grouted bolts in jointed rock and factors of influence. Rock Mech Rock Eng 23:201–229. https://doi.org/10.1007/BF01022954

Srivastava LP, Singh M (2015) Effect of fully grouted passive bolts on joint shear strength parameters in a blocky mass. Rock Mech Rock Eng 48:1197–1206. https://doi.org/10.1007/s00603-014-0615-8

Taheri A, Tani K (2010) Assessment of the stability of rock slopes by the slope stability rating classification system. Rock Mech Rock Eng 43:321–333. https://doi.org/10.1007/s00603-009-0050-4

Tang ZC, Huang RQ, Liu QS, Wong LNY (2016) Effect of contact state on the shear behavior of artificial rock joint. Bull Eng Geol Environ 75:761–769. https://doi.org/10.1007/s10064-015-0776-z

Thirukumaran S, Indraratna B, Brown ET, Kaiser PK (2016) Stability of a rock block in a tunnel roof under constant normal stiffness conditions. Rock Mech Rock Eng 49:1587–1593. https://doi.org/10.1007/s00603-015-0770-6

Wang G, Zhang Y, Jiang Y, Liu P, Guo Y, Liu J, Ma M, Wang K, Wang S (2018) Shear behaviour and acoustic emission characteristics of bolted rock joints with different roughnesses. Rock Mech Rock Eng. https://doi.org/10.1007/s00603-018-1438-9

Wang F, Cao P, R-h C, X-g X, Hao J (2019) The influence of temperature and time on water-rock interactions based on the morphology of rock joint surfaces. Bull Eng Geol Environ 78:3385–3394. https://doi.org/10.1007/s10064-018-1315-5

Wu X, Jiang Y, Li B (2018) Influence of joint roughness on the shear behaviour of fully encapsulated rock bolt. Rock Mech Rock Eng 51:953–959. https://doi.org/10.1007/s00603-017-1365-1

Yang ZY, Chiang DY (2000) An experimental study on the progressive shear behavior of rock joints with tooth-shaped asperities. Int J Rock Mech Min Sci 37:1247–1259. https://doi.org/10.1016/S1365-1609(00)00055-1

Zhang B, Li S, Xia K, Yang X, Zhang D, Wang S, Zhu J (2016) Reinforcement of rock mass with cross-flaws using rock bolt. Tunn Undergr Space Technol 51:346–353. https://doi.org/10.1016/j.tust.2015.10.007